

MSED: a multi-modal sleep event detection model for clinical sleep analysis

Alexander Neergaard Olesen, *Member, IEEE*, Poul Jennum,

Emmanuel Mignot, and Helge B. D. Sorensen, *Senior Member, IEEE*

January 8, 2021

Abstract

Study objective: Clinical sleep analysis require manual analysis of sleep patterns for correct diagnosis of sleep disorders. Several studies show significant variability in scoring discrete sleep events. We wished to investigate, whether an automatic method could be used for detection of arousals (Ar), leg movements (LM) and sleep disordered breathing (SDB) events, and if the joint detection of these events performed better than having three separate models.

Methods: We designed a single deep neural network architecture to jointly detect sleep events in a polysomnogram. We trained the model on 1653 recordings of individuals, and tested the optimized model on 1000 separate recordings. The performance of the model was quantified by F1, precision, and recall scores, and by correlating index values to clinical values using Pearson's correlation coefficient.

Results: F1 scores for the optimized model was 0.70, 0.63, and 0.62 for Ar, LM, and SDB, respectively. The performance was higher, when detecting events jointly compared to corresponding single-event models. Index values computed from detected events correlated well with manual annotations ($r^2 = 0.73$, $r^2 = 0.77$, $r^2 = 0.78$, respectively).

Conclusion: Detecting arousals, leg movements and sleep disordered breathing events jointly is possible, and the computed index values correlates well with human annotations.

1 Introduction

Clinical sleep analysis is currently performed manually by experts based on guidelines from the American Academy of Sleep Medicine (AASM) detailed in the AASM Scoring Manual [1]. The guidelines detail

both technical and clinical best practices for setting up and recording polysomnographies (PSGs), which are overnight recordings of various electrophysiological signals, such as electroencephalography (EEG), electrooculography (EOG), chin and leg electromyography (EMG), electrocardiography (ECG), respiratory inductance plethysmography from the thorax and abdomen, oronasal pressure, and blood oxygen levels.

Based on these signals, expert technicians analyse and score the PSG for sleep stages [wakefulness (W), rapid eye movement (REM) sleep, non-REM stage 1 (N1), non-REM stage 2 (N2), and non-REM stage 3 (N3)], and sleep micro-events summarized in key metrics, such as the apnea-hypopnea index (AHI) (number of apneas and hypopneas per hour of sleep), the periodic leg movement index (PLMI) (number of period leg movements per hour of sleep), and the arousal index (ArI) (number of arousals per hour of sleep).

Arousals are defined as abrupt shifts in EEG frequencies towards alpha, theta, and beta rhythms for at least 3s with a preceding period of stable sleep of at least 10s. During REM sleep, where the background EEG shows similar rhythms, arousal scoring requires a concurrent increase in chin EMG lasting at least 1s. Limb movements (LMs) should be scored in the leg EMG channels, when there is an increase in amplitude of at least $8\mu\text{V}$ above baseline level with a duration between 0.5s to 10s. A periodic leg movement (PLM) series is then defined as a sequence of 4 LMs, where the time between LM onsets is between 5 min to 90 min. Apneas are generally scored when there is a complete ($\geq 90\%$ of pre-event baseline) cessation of breathing activity either due to a physical obstruction (obstructive apnea) or due to an underlying disruption in the central nervous system control (central apnea) for at least 10s. When the breathing is only partially reduced ($\geq 30\%$ of pre-event baseline) and the duration of the excursion is $\geq 10\text{s}$, the event is scored as a hypopnea if there is either a $\geq 4\%$ oxygen desaturation or a $\geq 3\%$ oxygen desaturation coupled with an arousal (Ar).

However, several studies have shown significant variability in the scoring of both sleep stages [2]–[8] and sleep micro-events [9]–[16]. This has prompted extensive research into automatic methods for classifying sleep stages in large-scale studies [17]–[24], while the research in automatic arousal [25]–[27] and LM [28] detection on a similar scale is limited. Biswal *et al.* recently proposed a model based on a combination of recurrent and convolutional neural networks, where the same architecture was used for sleep stage classification, AHI and limb movement index (LMI) prediction. They trained their model using 9000 PSG recordings and evaluated the performance on the three tasks on a held out test set containing 1000 PSGs. However, this model was trained in separate runs for each downstream task; furthermore, post-processing was performed on the event predictions (apneas, limb movements).

In this study, we introduce the multi-modal sleep event detection (MSED) model for joint detection of sleep micro-events, in this case Ars, sleep disordered breathing (SDB), and LMs. The model is based on recent advances in machine learning and challenges current state of the art methods by directly classifying and localizing sleep micro-events in the PSG signals at the same time.

Table 1: MrOS demographics by subset.

	$\mathcal{D}_{\text{TRAIN}}$	$\mathcal{D}_{\text{EVAL}}$	$\mathcal{D}_{\text{TEST}}$	p -value
n	1653	200	1000	-
Age, years	76.4 \pm 5.6 [67.0, 90.0]	76.8 \pm 5.4 [68.0, 90.0]	76.4 \pm 5.3 [67.0, 90.0]	0.404
BMI, kg s ⁻²	27.3 \pm 3.9 [16.0, 47.0]	27.0 \pm 3.6 [19.0, 40.0]	27.0 \pm 3.7 [17.0, 45.0]	0.247
TST, min	357.3 \pm 69.0 [54.0, 615.0]	354.0 \pm 69.1 [108.0, 503.0]	353.6 \pm 68.7 [62.0, 572.0]	0.312
SL, min	22.9 \pm 25.6 [1.0, 349.0]	21.6 \pm 23.0 [1.0, 135.0]	25.1 \pm 32.1 [1.0, 402.0]	0.284
REML, min	109.5 \pm 77.9 [0.0, 578.0]	103.5 \pm 70.0 [10.0, 413.0]	107.2 \pm 75.3 [3.0, 590.0]	0.466
WASO, min	116.7 \pm 67.1 [11.0, 462.0]	119.0 \pm 70.8 [15.0, 372.0]	112.9 \pm 65.0 [6.0, 458.0]	0.471
SE, %	75.9 \pm 12.1 [17.0, 97.0]	75.5 \pm 12.3 [37.0, 96.0]	76.4 \pm 11.8 [26.0, 98.0]	0.690
N1, %	6.8 \pm 4.1 [0.0, 31.0]	7.0 \pm 4.5 [0.0, 28.0]	6.9 \pm 4.7 [1.0, 58.0]	0.968
N2, %	62.7 \pm 9.5 [28.0, 89.0]	62.0 \pm 9.7 [30.0, 90.0]	62.8 \pm 10.0 [21.0, 95.0]	0.451
N3, %	11.4 \pm 9.0 [0.0, 55.0]	11.8 \pm 9.7 [0.0, 55.0]	11.1 \pm 9.0 [0.0, 57.0]	0.638
REM, %	19.2 \pm 6.5 [0.0, 44.0]	19.4 \pm 7.2 [0.0, 41.0]	19.3 \pm 6.7 [0.0, 42.0]	0.894
ArI, h ⁻¹	23.5 \pm 11.8 [3.0, 87.0]	23.4 \pm 11.0 [4.0, 77.0]	23.8 \pm 11.8 [4.0, 102.0]	0.661
AHI, h ⁻¹	13.5 \pm 13.9 [0.0, 83.0]	13.6 \pm 13.3 [0.0, 59.0]	14.2 \pm 15.5 [0.0, 89.0]	0.907
PLMI, h ⁻¹	35.4 \pm 37.1 [0.0, 233.0]	36.6 \pm 39.0 [0.0, 178.0]	36.0 \pm 37.7 [0.0, 175.0]	0.993

Significant p -values at significance level $\alpha = 0.05$ are highlighted in bold. BMI: body-mass index; TST: total sleep time; SL: sleep latency; REML: REM sleep latency; WASO: wake after sleep onset; SE: sleep efficiency; N1: non-REM stage 1; N2: non-REM stage 2; N3: non-REM stage 3; REM: rapid eye movement; ArI: arousal index; AHI: apnea-hypopnea index; PLMI: periodic leg movement index.

2 Data

We collected PSGs from the MrOS Sleep Study, an ancillary part of the larger Osteoporotic Fractures in Men Study. The main goal of the study is to research and discover connections between sleep disorders, skeletal fractures, and cardiovascular disease and mortality in community-dwelling older (>65 years) [29]–[31]. Of the original 5994 study participants, 3135 subjects were enrolled at one of six sites in the USA for a comprehensive sleep assessment, while 2909 of these underwent a full-night in-home PSG recording. The PSG studies were subsequently scored by certified sleep technicians. Sleep stages were scored into stages 1, 2, 3, 4 and REM, while stages 3 and 4 combined into slow wave sleep (SWS) according to R&K rules [32]. Arous were scored as abrupt increases in EEG frequencies lasting at least 3 s according to American Sleep Disorders Association (ASDA) rules [33]. Apneas were defined as complete or near complete cessation of airflow lasting more than 10 s with an associated 3% or greater SaO₂ desaturation, while hypopneas were based on a clear reduction in breathing of more than 30% deviation from baseline breathing lasting more than 10 s, and likewise associated with a greater than 3% SaO₂ desaturation. While the scoring criteria for scoring LMs are not explicitly available for the MrOS Sleep Study, the prevailing standard at the time of the study was to score LMs following an increase in leg EMG amplitude of more than 8 μ V above resting baseline levels for at least 0.5 s, but shorter than 10 s [34].

2.1 Subset demographics and partitioning

We used a total of 2853 PSG studies downloaded from the National Sleep Research Resource (NSRR) [35], [36], which we partitioned into a training set ($\mathcal{D}_{\text{TRAIN}}$, $n_{\text{train}} = 1653$), a validation set ($\mathcal{D}_{\text{EVAL}}$, $n_{\text{eval}} = 200$), and a final testing set ($\mathcal{D}_{\text{TEST}}$, $n_{\text{test}} = 1000$). Key demographics and PSG-related variables for each subset are shown as mean \pm standard deviation with range in parenthesis in Table 1.

2.1.1 Signal and events

For this study, we considered three PSG events: Ars, LMs, and SDB events, which includes all forms of apneas (obstructive and central) and hypopneas. These event types are each based on a specific set of electrophysiological channels from the PSG, and as such, we extracted left and right central EEG (C3 and C4), left and right EOG, left and right chin EMG, left and right leg EMG, nasal pressure, and respiratory inductance plethysmography from the thorax and abdomen. EEG and EOG channels were referenced to the contralateral mastoid process, while a chin EMG was synthesized by subtracting the right chin EMG from the left chin EMG.

Apart from the raw signal data, we also extracted onset time relative to the study start time and duration times for each event type in each PSG.

3 Methods

Notation We denote by $\llbracket a, b \rrbracket$ the set of integers $\{n \in \mathbb{N} \mid a \leq n \leq b\}$ with $\llbracket N \rrbracket$ being shorthand for $\llbracket 1, N \rrbracket$, and by $n \in \llbracket N \rrbracket$ the n th sample in $\llbracket N \rrbracket$. A segment of PSG data is denoted by $\mathbf{x} \in \mathbb{R}^{C \times T}$, where C, T is the number of channels and the duration of the segment in samples, respectively. The corresponding set of N_t true events for the segment is denoted by $\boldsymbol{\varepsilon}^t = \{(\varrho_i^t, \delta_i^t) \in \mathbb{R}_+^2 \mid i \in \llbracket N_t \rrbracket\}$, where ϱ, δ are the center point and duration, respectively, of the i th event. By $\chi \in \mathcal{D}_*$ we denote a sample in either one of the three subsets. In the description of the network architecture, we have omitted the batch dimension from all calculations for brevity.

3.1 Model overview

Given an input set $\boldsymbol{\chi} = \{\mathbf{x}, \boldsymbol{\varepsilon}^t\} \in \mathbb{R}^{C \times T} \times \mathbb{R}_+^{N_t \times 2}$ containing PSG data with C channels and T time steps, and true events $\boldsymbol{\varepsilon}$, the goal of the model is to detect any possible events in the segment, where, in this context, detection covers both classification *and* localization of any event in the segment space.

To accomplish this, the model generates a set of *default event windows* $\boldsymbol{\varepsilon}^d = \{(\varrho_j^d, \delta_j^d) \in \mathbb{R}_+^2 \mid j \in \llbracket N_d \rrbracket\}$ for the current segment, and match each true event to a default event window if their intersection-over-union (IoU) is at least 0.5.

At test time, we generate predictions over the default event windows and use a non-maximum suppression procedure to select between the candidate predictions. For a given class k , the procedure is as follows. First, the predictions are sorted according to probability of the event, which is above a threshold θ_k . Then, using the most probable prediction as an anchor, we sequentially evaluate the IoU between the anchor and the remaining candidate predictions, removing those with $\text{IoU} \geq 0.5$.

The output of the model is thus the set $\{\mathbf{p}, \mathbf{y}\}$ containing the predicted class probabilities along with the corresponding onsets and durations.

3.2 Signal conditioning

We resampled all signals to a common sampling frequency of $f_s = 128$ Hz using a poly-phase filtering approach (Kaiser window, $\beta = 5.0$). Based on recommended filter specifications from the AASM, we designed Butterworth IIR filters for four sets of signals. EEG and EOG channels were filtered with a 2nd order filter with a 0.3 Hz–35 Hz passband, while chin and leg EMG channels were filtered with a 4th order high-pass filter with a 10 Hz cut-off frequency. The nasal pressure channel was filtered with a 4th order high-pass filter with a 0.03 Hz cut-off frequency, while the thoracoabdominal channels were filtered with a 2nd order with a 0.1 Hz–15 Hz passband.

All filters were implemented using the zero-phase method, which sequentially applies the filter in the forward direction, and then in the backwards direction. This accounts for the non-linear phase response and subsequent frequency-dependent group delay inherent in IIR filters, but also effectively squares the magnitude response of the filter.

Filtered signals were subsequently standardized by

$$\mathbf{x}^{(i)} = \frac{\hat{\mathbf{x}}^{(i)} - \boldsymbol{\mu}^{(i)}}{\boldsymbol{\sigma}^{(i)}}, \quad (1)$$

where $\hat{\mathbf{x}}^{(i)} \in \mathbb{R}^{C \times T}$ is the raw matrix containing C input channels and T samples, and $\boldsymbol{\mu}^{(i)}, \boldsymbol{\sigma}^{(i)} \in \mathbb{R}^C$ are the mean and standard deviation vectors for the i th PSG, respectively. This is a common approach in computer vision tasks, and beneficial to ensure a proper gradient propagation through a deep neural network [37].

3.3 Target encoding

For each data segment, target event classes $\boldsymbol{\pi} \in \mathbb{R}^{N_m \times K}$ generated by one-hot encoding, while the target detection variable containing the onset and duration times $\mathbf{t} \in \mathbb{R}^{N_m \times 2}$ was encoded as

$$t_i = \left(\frac{\varrho_i^m - \varrho_j^d}{\delta_j^d}, \log \frac{\delta_i^m}{\delta_j^d} \right), \quad i \in \llbracket N_m \rrbracket, j \in \llbracket N_d \rrbracket, \quad (2)$$

where ϱ_i^m is the center point of the true event matched to a default event window ϱ_j^d , and δ_i^m and δ_j^d are the corresponding durations of the true and default events.

3.4 Data sampling

As the total number of default event windows in a data segment N_d most likely will be much higher than the number of event windows matched to a true event, i. e. $N_d \gg N_m$, we implemented a similar random data sampling strategy as in [25]. At training step t , a given PSG record r has a certain number of associated number of Ar, LM, and SDB events (n_{Ar}, n_{LM}, n_{SDB} , respectively). We randomly sample a class k with equal probability $p_k = \frac{1}{K}$, whilst disregarding the negative class, since this class is most likely over-represented in the data segment. Given the class k , we randomly sample an event ε_k with probability $p(\varepsilon_k) \propto n_k$, and afterwards, we extract a segment of data of size $C \times T$, where the start of the segment is sampled from $[\bar{\varepsilon}_k - T, \bar{\varepsilon}_k + T]$, where $\bar{\varepsilon}_k$ is the sample midpoint of the event ε_k , thereby ensuring at least 50% overlap with at least one event associated with the data segment.

We found that this approach to sampling data segments with a large ratio of negative to positive samples to be beneficial in all our experiments, when monitoring the loss on the validation set.

3.5 Network architecture

Similar to the architecture described in [27], we designed a splitstream network architecture for the differentiable function Φ , where each stream is responsible for the bulk feature extraction for a specific event class. For the given problem of detecting Ars, LMs, and SDBs, the network contains three streams: the Ar stream takes as input the EEGs, the EOGs, and the chin EOG signals for a total of $C_{Ar} = 5$ channels; the LM stream receives the $C_{LM} = 2$ leg EMG signals; and the SDB stream receives the nasal pressure and the thoracoabdominal signals for a total of $C_{SDB} = 3$ channels. An overview of the network architecture is shown graphically in Figure 1.

3.5.1 Stream specifics

Each stream is comprised of two components. First, a mixing module $\varphi_{\text{mix}} : \mathbb{R}^{C_* \times T} \rightarrow \mathbb{R}^{C_* \times T}$ computes a non-linear mixing of the C channels using a set of C single-strided 1-dimensional filters $\mathbf{w} \in \mathbb{R}^{C \times C}$ and rectified linear unit (ReLU) activation [38], such that $\varphi_{\text{mix}}(\mathbf{x}) = \max\{0, \mathbf{w} \otimes \mathbf{x} + \mathbf{b}\}$, where the max operation introduces the non-linearity, \otimes is the conv operator over the C feature maps, and $\mathbf{b} \in \mathbb{R}^C$ is a bias vector (in this case $\mathbf{b} = 0$). Second, the output activations from φ_{mix} are used as input to a deep neural network module $\varphi_{\text{feat}} : \mathbb{R}^{C_* \times T} \rightarrow \mathbb{R}^{f' \times T'}$, which transforms the input feature maps to a $f' \times T'$ feature space with a temporal dimension reduced by a factor of $\frac{T}{T'}$. The feature extraction module φ_{feat} is realized using k_{max} successive conv operations with an increasing number of filters $f' = f_0 2^{k-1}$, $k \in \llbracket k_{\text{max}} \rrbracket$, where f_0 is a tunable base filter number. Each conv feature map is normalized

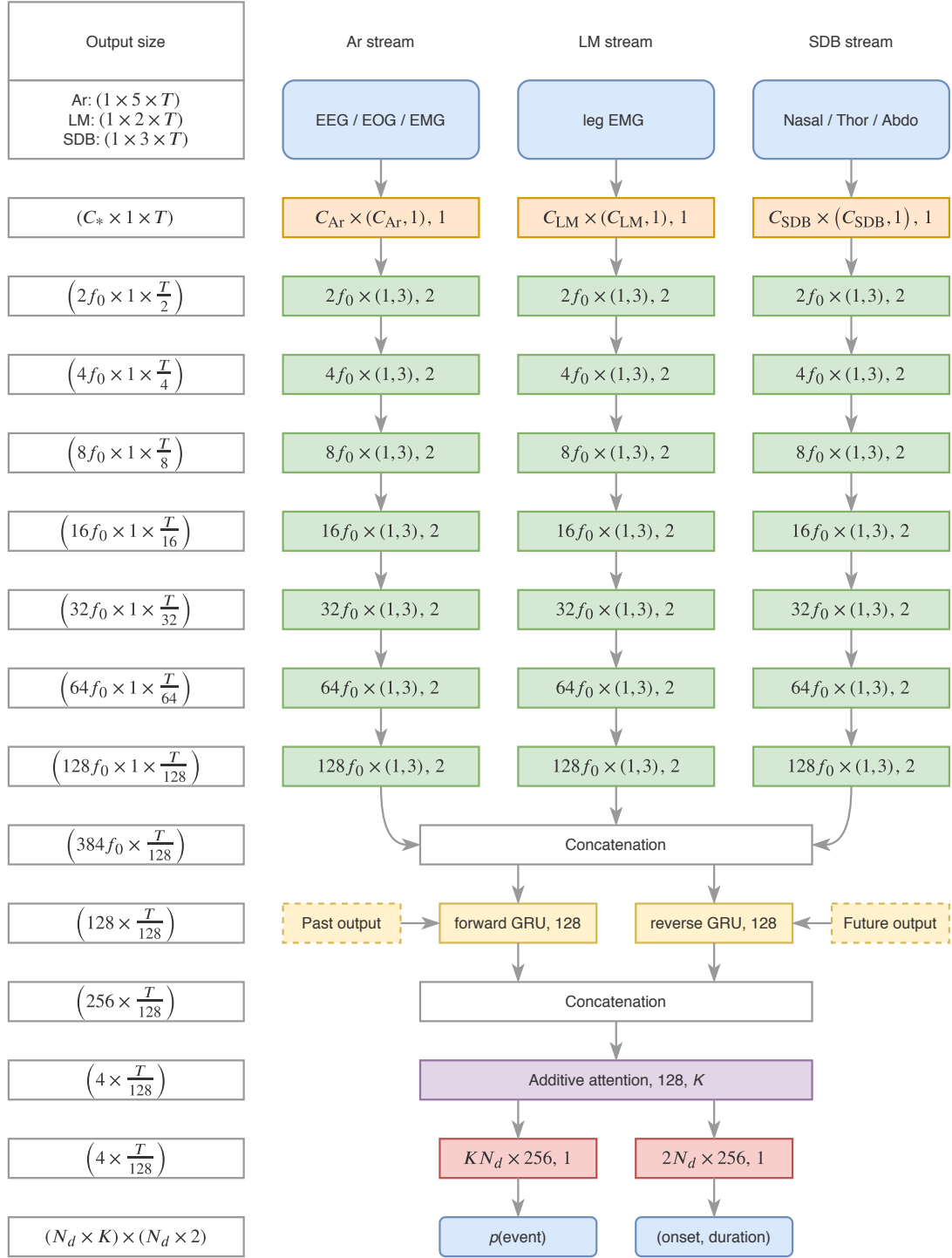


Figure 1: MSED network architecture. The left column shows the output dimensions for each operation as (number of filters [x singleton] x time steps). Each stream on the right (green) processes a separate set of input channels (blue, top), the results of which are concatenated before the bidirectional gated recurrent unit (bGRU) (yellow). The outputs from the additive attention layer (purple) are convolved in the final classification and localization layers (red) to output the probabilities for each event class, and the predicted onset and duration of each event (blue, bottom). Convolution layers (orange, green, red) are detailed as [number of feature maps x kernel size, stride]. Recurrent layer (yellow) shows the direction and number of hidden units. Additive attention layer (purple) is described with the number of hidden and output units.

using batch normalization (BN) [39], such that if $\tilde{\mathbf{z}} \in \mathbb{R}^{f' \times T'}$ denotes the output from a conv operation, the subsequent normalized version is computed as

$$\mathbf{z} = \gamma \frac{\tilde{\mathbf{z}} - \mathbb{E}[\tilde{\mathbf{z}}]}{\sqrt{\text{Var}[\tilde{\mathbf{z}}] + \epsilon}} + \beta, \quad (3)$$

where $\mathbb{E}[\tilde{\mathbf{z}}] \in \mathbb{R}^{f'}$, $\text{Var}[\tilde{\mathbf{z}}] \in \mathbb{R}_+^{f'}$ is the expectation and variance over the temporal dimension of each feature map, ϵ is a small constant, and $\{\gamma, \beta\} \in \mathbb{R}^{f'} \times \mathbb{R}^{f'}$ are learnable parameters representing the mean and bias for each feature map. Each normalized conv output is subsequently activated using ReLU.

3.5.2 Feature fusion for sequential processing

The outputs from the three feature extraction streams are subsequently fused by concatenating each output vector \mathbf{z}_* into a combined feature vector $\mathbf{z} = (\mathbf{z}_{\text{ar}}, \mathbf{z}_{\text{lm}}, \mathbf{z}_{\text{sdb}}) \in \mathbb{R}^{3f' \times T'}$. We introduce sequential modeling of the feature vectors using a bGRU [40], which has the advantage over other recurrent neural network (RNN)-based models such as the long short-term memory (LSTM) of having fewer trainable parameters while still being powerful enough to model complex, temporal relationships [41]. The output of the gated recurrent unit (GRU) for timestep t is a vector $\mathbf{h}_t = (\mathbf{h}_t^f, \mathbf{h}_t^b) \in \mathbb{R}^{2n_h}$ containing the concatenated outputs from the forward (f) and backward (b) directions. Each directional feature vector is calculated as a weighted combination of a gated new input \mathbf{n}_t and the feature vector from the previous timestep \mathbf{h}_{t-1}

$$\mathbf{h}_t^* = (1 - \mathbf{u}_t) \otimes \mathbf{n}_t + \mathbf{u}_t \otimes \mathbf{h}_{t-1}. \quad (4)$$

The update gate \mathbf{u}_t and gated new input \mathbf{n}_t are computed as

$$\mathbf{u}_t = \sigma(\mathbf{W}_u^z \mathbf{z}_t + \mathbf{b}_u^z + \mathbf{W}_u^h \mathbf{h}_{t-1} + \mathbf{b}_u^h), \quad (5)$$

$$\mathbf{n}_t = \tanh(\mathbf{W}_n^z \mathbf{z}_t + \mathbf{b}_n^z + \mathbf{r}_t \otimes (\mathbf{W}_n^h \mathbf{h}_{t-1} + \mathbf{b}_n^h)), \quad (6)$$

where \mathbf{W}_*^* , \mathbf{b}_*^* are weight matrices and bias vectors, respectively, and \mathbf{r}_t is a reset gate computed as

$$\mathbf{r}_t = \sigma(\mathbf{W}_r^z \mathbf{z}_t + \mathbf{b}_r^z + \mathbf{W}_r^h \mathbf{h}_{t-1} + \mathbf{b}_r^h). \quad (7)$$

3.5.3 Additive attention

The attention mechanism is a powerful technique to introduce a way for the network to focus on relevant regions and disregard irrelevant regions of a data sample, and is a key part of the highly successful Transformer model [42] and the subsequent state-of-the-art BERT model for natural language processing [43]. In this work, we implemented a simple, but powerful, *additive attention* mechanism [44], which computes *context*-vectors $\mathbf{c} \in \mathbb{R}^{2n_h}$ for each event class as the weighted sum of the feature vector

outputs $\mathbf{h} \in \mathbb{R}^{2n_h \times T'}$ from the φ_h . Formally, attention is computed as

$$\mathbf{c} = \mathbf{h} \cdot \boldsymbol{\alpha} = \sum_{t=1}^{T'} \mathbf{h}_t \boldsymbol{\alpha}_t, \quad (8)$$

where T' is the reduced temporal dimension, \mathbf{h}_t is the feature vector for time step t , and $\boldsymbol{\alpha}_t \in \mathbb{R}^K$ is the attention weight computed as

$$\boldsymbol{\alpha}_t = \frac{\exp(\tanh(\mathbf{h}_t \mathbf{W}_u) \mathbf{W}_a)}{\sum_{\tau} \exp(\tanh(\mathbf{h}_{\tau} \mathbf{W}_u) \mathbf{W}_a)}. \quad (9)$$

Here, $\mathbf{W}_u \in \mathbb{R}^{2n_h \times n_a}$ and $\mathbf{W}_a \in \mathbb{R}^{n_a \times K}$ are linear mappings of the feature vectors, and \tanh is the hyperbolic tangent function.

3.5.4 Detection

The final event classification and localization is handled by two modules, $\psi_{\text{clf}} : \mathbb{R}^{2n_h \times K} \rightarrow \mathbb{R}^{N_d \times K}$ and $\psi_{\text{loc}} : \mathbb{R}^{2n_h \times K} \rightarrow \mathbb{R}^{N_d \times 2}$, respectively. The classification module $\psi_{\text{clf}} : \mathbf{c} \mapsto \mathbf{p}$ outputs a tensor $\mathbf{p} \in [0, 1]_+^{N_d \times K}$ containing predicted event class probabilities for each default event window. The localization module $\psi_{\text{loc}} : \mathbf{c} \mapsto \mathbf{y}$ outputs a tensor $\mathbf{y} \in \mathbb{R}^{N_d \times 2}$ containing encoded relative onsets and durations for a detected event for each default event window.

3.6 Loss function

Similar to [45], we optimized the network parameters according to a three-component loss function consisting of: i) a localization loss ℓ_{loc} ; ii) a positive classification loss ℓ_+ , and iii) a negative classification loss ℓ_- , such that the total loss ℓ was defined by

$$\ell = \ell_{\text{loc}} + \ell_+ + \ell_-. \quad (10)$$

The localization loss ℓ_{loc} was calculated using a Huber function

$$\ell_{\text{loc}} = \frac{1}{N_+} \sum_{i \in \pi_+} f_H^{(i)} \quad (11)$$

$$\mathbf{f}_H = \begin{cases} 0.5(\mathbf{y} - \mathbf{t})^2, & \text{if } |\mathbf{y} - \mathbf{t}| < 1, \\ |\mathbf{y} - \mathbf{t}| - 0.5, & \text{otherwise,} \end{cases} \quad (12)$$

where $i \in \pi_+$ yields indices of event windows with positive targets, i.e. event windows matched to an arousal, LM or SDB target, and N_+ is the number of positive targets in the given data segment.

The positive classification loss component ℓ_+ was calculated using a simple cross-entropy over the

event windows matched to an arousal, LM, or SDB event:

$$\ell_+ = \frac{1}{N_+} \sum_{i \in \pi_+} \sum_{k \in \llbracket K \rrbracket} \pi_k^{(i)} \log p_k^{(i)}, \quad \text{where} \quad p_k^{(i)} = \frac{\exp s_k^{(i)}}{\sum_j \exp s_j^{(i)}}, \quad (13)$$

and $\pi_k^{(i)}$, $p_k^{(i)}$, and $s_k^{(i)}$ are the true class probability, predicted class probability, and logit score for the i th event window containing a positive sample.

Similar to [46], [47], the negative classification loss ℓ_- was calculated using a hard negative mining approach to balance the number of positive and negative samples in a data segment after matching default event windows to true events [48]. Specifically, this is accomplished by calculating the probability for the negative class (no event) for each unmatched default event window, and then calculating the cross entropy loss using the Z most probable samples. In our experiments, we set the ratio of positive to negative samples as 1:3, such that the calculation of ℓ involves $Z = 3$ times as many negative as positive samples.

We also explored a focal loss objective function for computing ℓ_+ and ℓ_- [49], however, we found that this approach severely deteriorated the ability of the network to accurately detect LM and SDB events compared to using worst negative mining.

3.7 Optimization

The network parameters were optimized using adaptive moment estimation (Adam) according to the loss function described in Equation (10) [50]. This algorithm uses first (m) and second (v) moment estimations of gradients to update the model parameters θ of a differentiable function f at time t :

$$m^{(t)} = \beta_1 m^{(t-1)} + (1 - \beta_1) \nabla_{\theta} f^{(t)}(\theta^{(t-1)}) \quad (14)$$

$$v^{(t)} = \beta_2 v^{(t-1)} + (1 - \beta_2) \nabla_{\theta}^2 f^{(t)}(\theta^{(t-1)}), \quad (15)$$

where β_1, β_2 are exponential decay rates for the first and second moment, respectively, ∇ is the gradient vector with respect to θ , and ∇_{θ}^2 is the Hadamard product $\nabla_{\theta} f \odot \nabla_{\theta} f$. The moment vectors are initialized with 0's, which induce a bias towards zero. This can be offset by computing a bias-corrected estimate of each moment vector as

$$\hat{m}^{(t)} = \frac{m^{(t)}}{1 - \beta_1^t} \quad (16)$$

$$\hat{v}^{(t)} = \frac{v^{(t)}}{1 - \beta_2^t}, \quad (17)$$

which yields the final update to θ as

$$\theta^{(t)} = \theta^{(t-1)} - \eta \frac{\hat{m}^{(t)}}{\sqrt{\hat{v}^{(t)} + \epsilon}}, \quad (18)$$

where η is the learning rate.

3.8 Experimental setups

In our experiments, we fixed the exponential decay rates at $(\beta_1, \beta_2) = (0.9, 0.999)$, the learning rate at $\eta = 10^{-3}$, and $\epsilon = 10^{-8}$. The learning rate was decayed in a step-wise manner by multiplying η with a factor of 0.1 after 3 consecutive epochs with no improvement in loss value on the validation dataset.

Similarly, we employed an early stopping scheme by monitoring the loss on the validation dataset and stopping the model training after 10 epochs of no improvement on $\mathcal{D}_{\text{EVAL}}$.

We tested four types of models in two categories: the first is a default split-stream model as shown in Figure 1 with and without weight decay (splitstream, splitstream-wd). The second is a variation of the split-stream model, but where the ψ_{cif} and ψ_{loc} modules are realized using depth-wise convolutions, such that each attention group is used only for that type of event. The second category is also tested with and without weight decay (splitstream-dw, splitstream-dw-wd).

3.9 Performance evaluation

Performance was quantified using precision, recall and F1 scores. Statistical significance in F1 score between groups was assessed with Kruskal-Wallis H -tests. The performance of joint vs. single-event detection models was tested with Wilcoxon signed rank tests for matched samples. The relationships between true and predicted ArI, AHI, and LMI were assessed using linear models and Pearsons r^2 . Significance was set at $\alpha = 0.05$.

4 Results and discussion

4.1 Model architecture evaluation

We found no significant differences in F1 performance for either Ar (Kruskal-Wallis $H = 0.961$, $p = 0.811$), LM ($H = 0.230$, $p = 0.973$), or SDB detection ($H = 2.838$, $p = 0.417$), when evaluating the model architectures on $\mathcal{D}_{\text{EVAL}}$ (see Figure 2). Based on this result, all further modeling was based on the default splitstream architecture for simplicity.

4.2 Joint vs. single event detection

For each event type, we evaluated the F1 score as a function of classification threshold θ on $\mathcal{D}_{\text{EVAL}}$ for both the joint detection model as well as the single-event models. It can be observed in Figure 3 that for all three events, the joint detection model achieves higher F1 score, although the apparent increase is not as large for LM detection. This was also observed when evaluating the joint and single detection

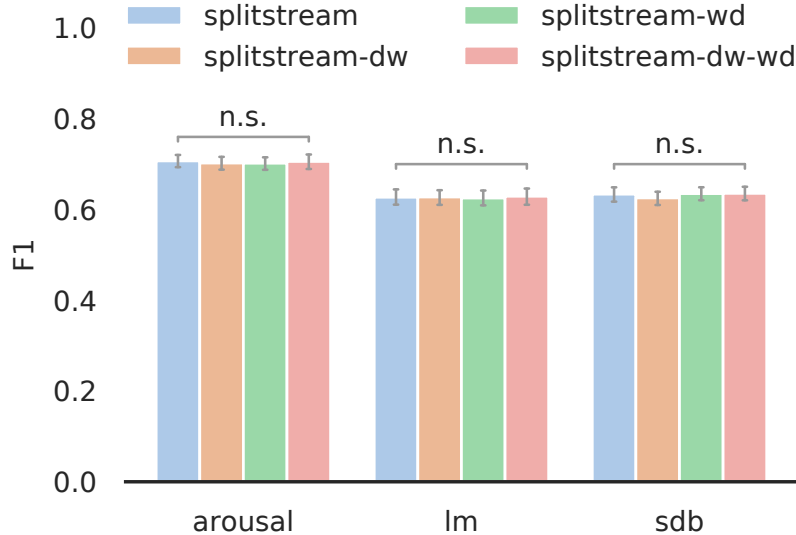


Figure 2: Architecture optimization.

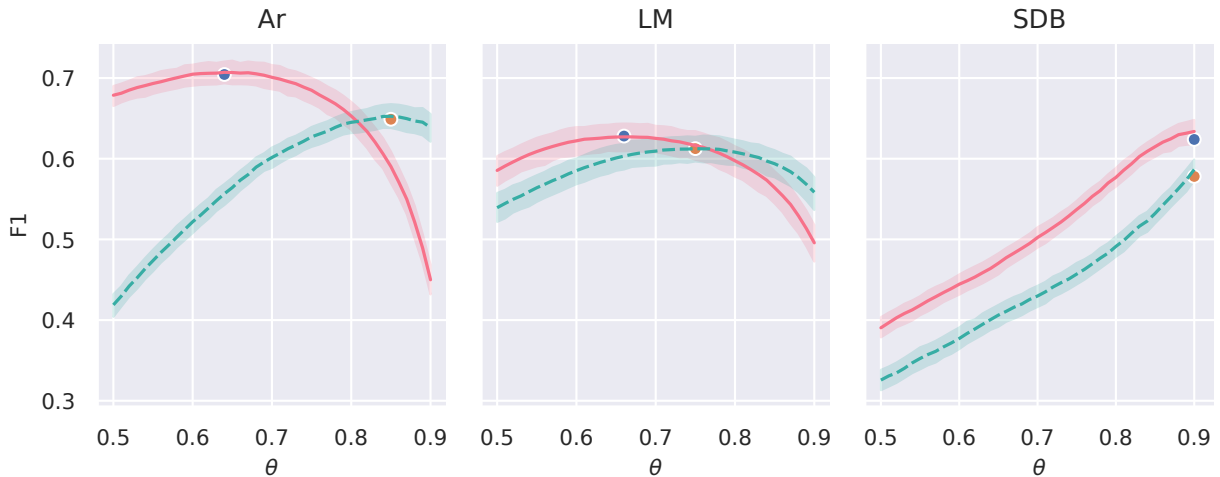


Figure 3: Optimizing F1 performance on $\mathcal{D}_{\text{EVAL}}$ as a function of θ). Full lines correspond to the joint model and dashed lines are the corresponding single-event detection model. The blue and orange dots correspond to optimized model performance on $\mathcal{D}_{\text{TEST}}$.

models with optimized thresholds on $\mathcal{D}_{\text{TEST}}$ for both Ar (Wilcoxon $W = 30440.0$, $p = 2.481 \times 10^{-127}$), LM ($W = 101103.0$, $p = 6.454 \times 10^{-60}$), and SDB detection ($W = 93647.0$, $p = 2.378 \times 10^{-64}$). Precision, recall and F1 scores for optimized models evaluated on $\mathcal{D}_{\text{TEST}}$ are shown in Table 2. These findings are interesting, because they provide evidence that the presence of different event types can modulate the detection of others, and that this can be modeled using automatic methods. This is in line with what previous studies have found e.g. on event-by-event scoring agreement in arousals, which improved significantly from 0.59 % to 0.91 %, when including respiratory signals in the analysis [13].

4.2.1 Detection vs. manual scorings

For each event type, we computed the correlation coefficient between the predicted and true index values (arousal index, ArI; apnea-hypopnea index, AHI; limb movement index, LMI), which is shown

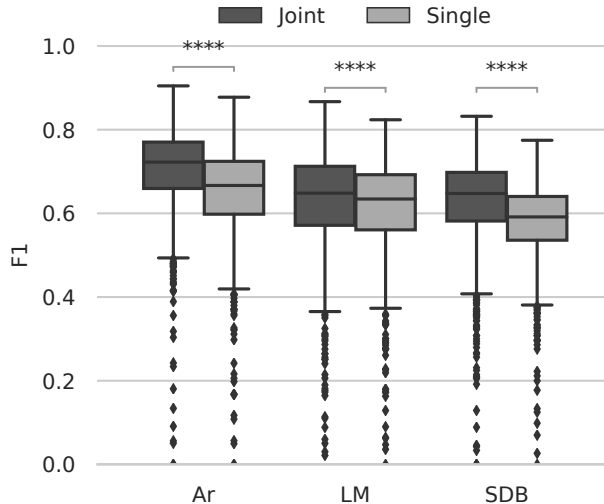


Figure 4: Evaluating optimized joint and single-event detection models on $\mathcal{D}_{\text{TEST}}$. ****: $p < 10 \times 10^{-4}$. Ar: arousal; LM: limb movement; SDB: sleep disordered breathing.

Table 2: Performance scores for optimized models evaluated on $\mathcal{D}_{\text{TEST}}$.

Event	Model	Precision	Recall	F1
Ar	Joint	0.759 ± 0.114	0.672 ± 0.125	0.704 ± 0.106
	Single	0.777 ± 0.107	0.571 ± 0.127	0.649 ± 0.113
LM	Joint	0.650 ± 0.169	0.647 ± 0.120	0.628 ± 0.123
	Single	0.661 ± 0.166	0.607 ± 0.116	0.613 ± 0.116
SDB	Joint	0.817 ± 0.142	0.526 ± 0.146	0.624 ± 0.115
	Single	0.765 ± 0.142	0.486 ± 0.121	0.578 ± 0.097

Metrics are shown aggregated across PSGs. Ar: arousal; LM: limb movement; SDB: sleep disordered breathing.

in Figure 5. We found a large positive correlation between true and predicted values for ArI ($r^2 = 0.73$, $p = 2.5 \times 10^{-285}$), AHI ($r^2 = 0.77$, $p = 9.3 \times 10^{-316}$), and LMI ($r^2 = 0.78$, $p = 3.1 \times 10^{-321}$).

A similar study using an automatic method for automatic detection of SDB and LM events found similar or higher correlations between automatic and manual scorings ($r^2 = 0.85$, and $r^2 = 0.79$, respectively), although their findings were based on almost 5 times as much data [21]. Furthermore, obstructive, central, mixed and hypopneas with an associated 4% desaturation were lumped together in one single *apnea* class, which may have biased their findings towards obstructive apneas and hypopneas, since these are in general more prevalent than central and mixed apneas.

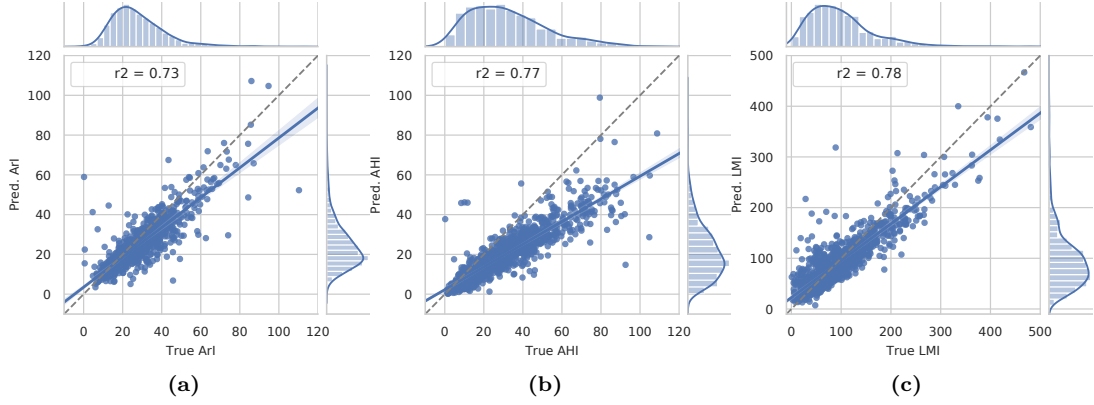


Figure 5: Pearson correlation plots for each event type index between true and predicted values. The linear relationship is indicated with solid blue with 95% confidence intervals in light blue. Grey dashed lines indicate perfect correlation lines. ArI: arousal index; AHI: apnea-hypopnea index; LMI: limb movement index.

4.2.2 Temporal characteristics

We compared the temporal precision between manual and automatic event scoring by looking at the errors in onset (Δ_{onset}), offsets (Δ_{offset}), and durations ($\Delta_{\text{dur.}}$) calculated as

$$\Delta_{\text{onset}} = \text{onset}_{\text{automatic}} - \text{onset}_{\text{manual}} \quad (19)$$

$$\Delta_{\text{offset}} = \text{offset}_{\text{automatic}} - \text{offset}_{\text{manual}} \quad (20)$$

$$\Delta_{\text{dur.}} = \text{dur}_{\text{automatic}} - \text{dur}_{\text{manual}} \quad (21)$$

so that positive values of Δ_{onset} , Δ_{offset} corresponds to a positive shift to the right (delayed prediction), and positive values of $\Delta_{\text{dur.}}$ meaning an overestimation of the event duration compared to manual scoring. This is shown in Figure 6, where the blue distributions are the joint detection model for each event type, and the orange distributions are the corresponding single-event models. The distributions are shown as kernel density estimates superimposed on a histogram. For Ar events, the model overestimates the duration on average by a couple of seconds, which is caused by an earlier prediction of onset and delayed prediction of termination. For LM events, the model underestimates the duration by about half a second on average, which is due to earlier prediction of termination. For SDB events, the model overestimates the duration by about 25 seconds on average, which is caused by an earlier prediction of onset and delayed prediction of termination. These errors in predicted durations reflects the temporal characteristics of these events; LMs are shorter events (between 0.5 s to 10 s per definition), and it is thus unlikely to be overestimated by several seconds, while SDBs are longer events by one to two orders of magnitude, which also increases the size of the errors. Ars events are intermediate in length compared to LMs and SDBs, which is reflected in the error distributions.

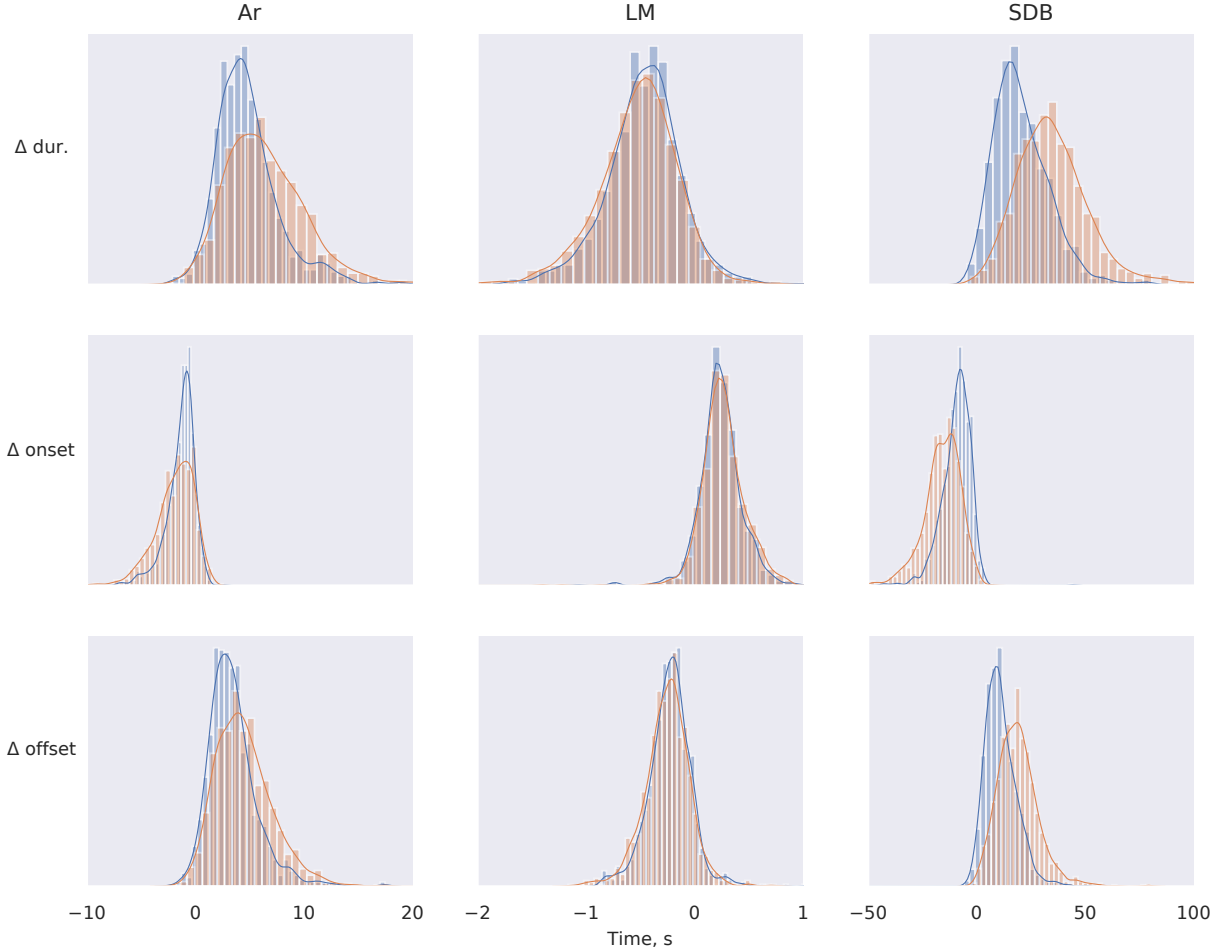


Figure 6: Temporal error metrics distributions across all events and PSGs. Positive values of Δ_{onset} , Δ_{offset} means delayed predictions, while positive values of $\Delta_{\text{dur.}}$ means to an overestimation of event duration. Blue distributions are joint detection models, while orange distributions are the corresponding single-event models. Distributions are shown as kernel density estimates superimposed on a histogram. Ar: arousal; LM: limb movement; SDB: sleep disordered breathing.

5 Conclusion

We have presented a novel method for detecting short and long events present in polysomnogram recordings based on deep neural networks. Our method was able to distinguish between arousals, limb movements, and sleep-disordered breathing events with F1 scores of 0.70, 0.63, and 0.62, respectively, and we furthermore found that jointly optimizing a model for all three events performed better than the respective models optimized for each specific event type.

Furthermore, clinically relevant event index values derived from the model outputs showed a high positive correlation with manually computed index values indicating a high degree of agreement between our model and humans.

References

- [1] R. B. Berry, R. Brooks, C. E. Gamaldo, S. M. Harding, C. L. Marcus, and B. V. Vaughn, *The AASM Manual for the Scoring of Sleep and Associated Events: Rules, Terminology and Technical Specifications, Version 2.6*. Darien, IL, USA: American Academy of Sleep Medicine, 2020.
- [2] R. G. Norman, I. Pal, C. Stewart, J. A. Walsleben, and D. M. Rapoport, “Interobserver Agreement Among Sleep Scorers From Different Centers in a Large Dataset,” *Sleep*, vol. 23, no. 7, pp. 1–8, 2000. DOI: [10.1093/sleep/23.7.1e](https://doi.org/10.1093/sleep/23.7.1e).
- [3] H. Danker-Hopfe, D. Kunz, G. Gruber, G. Klösch, J. L. Lorenzo, S. L. Himanen, B. Kemp, T. Penzel, J. Röschke, H. Dorn, A. Schlögl, E. Trenker, and G. Dorffner, “Interrater reliability between scorers from eight European sleep laboratories in subjects with different sleep disorders,” *J. Sleep Res.*, vol. 13, pp. 63–69, 2004. DOI: [10.1046/j.1365-2869.2003.00375.x](https://doi.org/10.1046/j.1365-2869.2003.00375.x).
- [4] H. Danker-Hopfe, P. Anderer, J. Zeitlhofer, M. Boeck, H. Dorn, G. Gruber, E. Heller, E. Loretz, D. Moser, S. Parapatics, B. Saletu, A. Schmidt, and G. Dorffner, “Interrater reliability for sleep scoring according to the Rechtschaffen & Kales and the new AASM standard,” *J. Sleep Res.*, vol. 18, no. 1, pp. 74–84, 2009. DOI: [10.1111/j.1365-2869.2008.00700.x](https://doi.org/10.1111/j.1365-2869.2008.00700.x).
- [5] R. S. Rosenberg and S. Van Hout, “The American Academy of Sleep Medicine Inter-scorer Reliability Program: Sleep Stage Scoring,” *J. Clin. Sleep Med.*, vol. 9, pp. 81–87, 2013. DOI: [10.5664/jcsm.2350](https://doi.org/10.5664/jcsm.2350).
- [6] X. Zhang, X. Dong, J. W. Kantelhardt, J. Li, L. Zhao, C. Garcia, M. Glos, T. Penzel, and F. Han, “Process and outcome for international reliability in sleep scoring,” *Sleep Breath.*, vol. 19, no. 1, pp. 191–195, 2015. DOI: [10.1007/s11325-014-0990-0](https://doi.org/10.1007/s11325-014-0990-0).
- [7] M. Younes, J. Raneri, and P. Hanly, “Staging sleep in polysomnograms: Analysis of inter-scorer variability,” *J. Clin. Sleep Med.*, vol. 12, no. 6, pp. 885–894, 2016. DOI: [10.5664/jcsm.5894](https://doi.org/10.5664/jcsm.5894).
- [8] M. Younes, S. T. Kuna, A. I. Pack, J. K. Walsh, C. A. Kushida, B. Staley, and G. W. Pien, “Reliability of the American Academy of Sleep Medicine Rules for Assessing Sleep Depth in Clinical Practice,” *J. Clin. Sleep Med.*, vol. 14, no. 2, pp. 205–213, 2018. DOI: [10.5664/jcsm.6934](https://doi.org/10.5664/jcsm.6934).
- [9] M. J. Drinnan, A. Murray, C. J. Griffiths, and G. J. Gibson, “Interobserver Variability in Recognizing Arousal in Respiratory Sleep Disorders,” *Am. J. Respir. Crit. Care Med.*, vol. 158, pp. 358–362, 1998. DOI: [10.1164/ajrccm.158.2.9705035](https://doi.org/10.1164/ajrccm.158.2.9705035).
- [10] C. W. Whitney, D. J. Gottlieb, S. Redline, R. G. Norman, R. R. Dodge, E. Shahar, S. Surovec, and F. J. Nieto, “Reliability of scoring respiratory disturbance indices and sleep staging,” *Sleep*, vol. 21, no. 7, pp. 749–757, 1998. DOI: [10.1093/sleep/21.7.749](https://doi.org/10.1093/sleep/21.7.749).

- [11] J. S. Lored, J. L. Clausen, S. Ancoli-Israel, and J. E. Dimsdale, “Night-to-Night Arousal Variability and Interscorer Reliability of Arousal Measurements,” *Sleep*, vol. 22, no. 7, pp. 916–920, 1999. DOI: [10.1093/sleep/22.7.916](https://doi.org/10.1093/sleep/22.7.916).
- [12] M. Smurra, M. Dury, G. Aubert, D. Rodenstein, and G. Liistro, “Sleep fragmentation: comparison of two definitions of short arousals during sleep in OSAS patients,” *Eur. Respir. J.*, vol. 17, pp. 723–727, 2001. DOI: [10.1183/09031936.01.17407230](https://doi.org/10.1183/09031936.01.17407230).
- [13] R. J. Thomas, “Arousals in Sleep-disordered Breathing: Patterns and Implications,” *Sleep*, vol. 26, no. 8, pp. 1042–1047, 2003. DOI: [10.1093/sleep/26.8.1042](https://doi.org/10.1093/sleep/26.8.1042).
- [14] M. H. Bonnet, K. Doghramji, T. Roehrs, E. J. Stepanski, S. H. Sheldon, A. S. Walters, M. Wise, and A. L. Chesson, “The scoring of arousal in sleep: Reliability, validity, and alternatives,” *J. Clin. Sleep Med.*, vol. 3, no. 2, pp. 133–145, 2007. DOI: [10.5664/jcsm.26815](https://doi.org/10.5664/jcsm.26815).
- [15] U. J. Magalang, N.-H. Chen, P. A. Cistulli, A. C. Fedson, T. Gíslason, D. Hillman, T. Penzel, R. Tamisier, S. Tufik, G. Phillips, and A. I. Pack, “Agreement in the Scoring of Respiratory Events and Sleep Among International Sleep Centers,” *Sleep*, vol. 36, no. 4, pp. 591–596, 2013. DOI: [10.5665/sleep.2552](https://doi.org/10.5665/sleep.2552).
- [16] R. S. Rosenberg and S. Van Hout, “The American Academy of Sleep Medicine Inter-scorer Reliability Program: Respiratory Events,” *J. Clin. Sleep Med.*, vol. 10, no. 4, pp. 447–454, 2014. DOI: [10.5664/jcsm.3630](https://doi.org/10.5664/jcsm.3630).
- [17] H. Koch, J. A. Christensen, R. Frandsen, M. Zoetmulder, L. Arvastson, S. R. Christensen, P. Jennum, and H. B. Sorensen, “Automatic sleep classification using a data-driven topic model reveals latent sleep states,” *J. Neurosci. Methods*, vol. 235, pp. 130–137, 2014. DOI: [10.1016/j.jneumeth.2014.07.002](https://doi.org/10.1016/j.jneumeth.2014.07.002).
- [18] A. Supratak, H. Dong, C. Wu, and Y. Guo, “DeepSleepNet: A Model for Automatic Sleep Stage Scoring Based on Raw Single-Channel EEG,” *IEEE Trans. Neural Syst. Rehabil. Eng.*, vol. 25, no. 11, pp. 1998–2008, 2017. DOI: [10.1109/TNSRE.2017.2721116](https://doi.org/10.1109/TNSRE.2017.2721116).
- [19] S. Chambon, M. N. Galtier, P. J. Arnal, G. Wainrib, and A. Gramfort, “A Deep Learning Architecture for Temporal Sleep Stage Classification Using Multivariate and Multimodal Time Series,” *IEEE Trans. Neural Syst. Rehabil. Eng.*, vol. 26, no. 4, pp. 758–769, 2018. DOI: [10.1109/TNSRE.2018.2813138](https://doi.org/10.1109/TNSRE.2018.2813138).
- [20] A. N. Olesen, P. Jennum, P. Peppard, E. Mignot, and H. B. D. Sorensen, “Deep residual networks for automatic sleep stage classification of raw polysomnographic waveforms,” in *2018 40th Annu. Int. Conf. IEEE Eng. Med. Biol. Soc.*, Honolulu, HI, USA: IEEE, 2018, pp. 1–4. DOI: [10.1109/EMBC.2018.8513080](https://doi.org/10.1109/EMBC.2018.8513080).

- [21] S. Biswal, H. Sun, B. Goparaju, M. B. Westover, J. Sun, and M. T. Bianchi, “Expert-level sleep scoring with deep neural networks,” *J. Am. Med. Informatics Assoc.*, vol. 25, no. 12, pp. 1643–1650, 2018. DOI: [10.1093/jamia/ocy131](https://doi.org/10.1093/jamia/ocy131).
- [22] J. B. Stephansen, A. N. Olesen, M. Olsen, A. Ambati, E. B. Leary, H. E. Moore, O. Carrillo, L. Lin, F. Han, H. Yan, Y. L. Sun, Y. Dauvilliers, S. Scholz, L. Barateau, B. Hogl, A. Stefani, S. C. Hong, T. W. Kim, F. Pizza, G. Plazzi, S. Vandi, E. Antelmi, D. Perrin, S. T. Kuna, P. K. Schweitzer, C. Kushida, P. E. Peppard, H. B. D. Sorensen, P. Jennum, and E. Mignot, “Neural network analysis of sleep stages enables efficient diagnosis of narcolepsy,” *Nat. Commun.*, vol. 9, no. 1, p. 5229, 2018. DOI: [10.1038/s41467-018-07229-3](https://doi.org/10.1038/s41467-018-07229-3).
- [23] H. Phan, F. Andreotti, N. Cooray, O. Y. Chen, and M. De Vos, “Joint Classification and Prediction CNN Framework for Automatic Sleep Stage Classification,” *IEEE Trans. Biomed. Eng.*, vol. 66, no. 5, pp. 1285–1296, 2019. DOI: [10.1109/TBME.2018.2872652](https://doi.org/10.1109/TBME.2018.2872652).
- [24] —, “SeqSleepNet: End-to-End Hierarchical Recurrent Neural Network for Sequence-to-Sequence Automatic Sleep Staging,” *IEEE Trans. Neural Syst. Rehabil. Eng.*, vol. 27, no. 3, pp. 400–410, 2019. DOI: [10.1109/TNSRE.2019.2896659](https://doi.org/10.1109/TNSRE.2019.2896659).
- [25] A. N. Olesen, S. Chambon, V. Thorey, P. Jennum, E. Mignot, and H. B. D. Sorensen, “Towards a Flexible Deep Learning Method for Automatic Detection of Clinically Relevant Multi-Modal Events in the Polysomnogram,” in *2019 41st Annu. Int. Conf. IEEE Eng. Med. Biol. Soc.*, Berlin, Germany: IEEE, 2019, pp. 556–561. DOI: [10.1109/EMBC.2019.8856570](https://doi.org/10.1109/EMBC.2019.8856570).
- [26] D. Alvarez-Estevéz and I. Fernández-Varela, “Large-scale validation of an automatic EEG arousal detection algorithm using different heterogeneous databases,” *Sleep Med.*, vol. 57, pp. 6–14, 2019. DOI: [10.1016/j.sleep.2019.01.025](https://doi.org/10.1016/j.sleep.2019.01.025).
- [27] A. Brink-Kjaer, A. N. Olesen, P. E. Peppard, K. L. Stone, P. Jennum, E. Mignot, and H. B. Sorensen, “Automatic Detection of Cortical Arousals in Sleep and their Contribution to Daytime Sleepiness,” *Clin. Neurophysiol.*, 2020. DOI: [10.1016/j.clinph.2020.02.027](https://doi.org/10.1016/j.clinph.2020.02.027). arXiv: [1906.01700](https://arxiv.org/abs/1906.01700) [q-bio.NC].
- [28] L. Carvelli, A. N. Olesen, A. Brink-Kjær, E. B. Leary, P. E. Peppard, E. Mignot, H. B. Sørensen, and P. Jennum, “Design of a deep learning model for automatic scoring of periodic and non-periodic leg movements during sleep validated against multiple human experts,” *Sleep Med.*, vol. 69, pp. 109–119, 2020. DOI: [10.1016/j.sleep.2019.12.032](https://doi.org/10.1016/j.sleep.2019.12.032).
- [29] J. B. Blank, P. M. Cawthon, M. L. Carrion-Petersen, L. Harper, J. P. Johnson, E. Mitson, and R. R. Delay, “Overview of recruitment for the osteoporotic fractures in men study (MrOS),” *Contemp. Clin. Trials*, vol. 26, no. 5, pp. 557–568, 2005. DOI: [10.1016/j.cct.2005.05.005](https://doi.org/10.1016/j.cct.2005.05.005).

- [30] E. Orwoll, J. B. Blank, E. Barrett-Connor, J. Cauley, S. Cummings, K. Ensrud, C. Lewis, P. M. Cawthon, R. Marcus, L. M. Marshall, J. McGowan, K. Phipps, S. Sherman, M. L. Stefanick, and K. Stone, “Design and baseline characteristics of the osteoporotic fractures in men (MrOS) study — A large observational study of the determinants of fracture in older men,” *Contemp. Clin. Trials*, vol. 26, no. 5, pp. 569–585, 2005. DOI: [10.1016/j.cct.2005.05.006](https://doi.org/10.1016/j.cct.2005.05.006).
- [31] T. Blackwell, K. Yaffe, S. Ancoli-Israel, S. Redline, K. E. Ensrud, M. L. Stefanick, A. Laffan, and K. L. Stone, “Associations Between Sleep Architecture and Sleep-Disordered Breathing and Cognition in Older Community-Dwelling Men: The Osteoporotic Fractures in Men Sleep Study,” *J. Am. Geriatr. Soc.*, vol. 59, no. 12, pp. 2217–2225, 2011. DOI: [10.1111/j.1532-5415.2011.03731.x](https://doi.org/10.1111/j.1532-5415.2011.03731.x).
- [32] A. Rechtschaffen and A. Kales, Eds., *A manual of standardized terminology, techniques and scoring system for sleep stages of human subjects*. Washington, DC: National Institute of Health, 1968.
- [33] American Sleep Disorders Association, “EEG arousals: scoring rules and examples: a preliminary report from the Sleep Disorders Atlas Task Force of the American Sleep Disorders Association,” *Sleep*, vol. 15, no. 2, pp. 173–184, 1992, PMID: [11032543](https://pubmed.ncbi.nlm.nih.gov/11032543/).
- [34] M. Zucconi, R. Ferri, R. Allen, P. C. Baier, O. Bruni, S. Chokroverty, L. Ferini-Strambi, S. Fulda, D. Garcia-Borreguero, W. A. Hening, M. Hirshkowitz, B. Högl, M. Hornyak, M. King, P. Montagna, L. Parrino, G. Plazzi, and M. G. Terzano, “The official World Association of Sleep Medicine (WASM) standards for recording and scoring periodic leg movements in sleep (PLMS) and wakefulness (PLMW) developed in collaboration with a task force from the International Restless Legs Syndrome Study Group,” *Sleep Med.*, vol. 7, no. 2, pp. 175–183, 2006. DOI: [10.1016/j.sleep.2006.01.001](https://doi.org/10.1016/j.sleep.2006.01.001).
- [35] D. A. Dean, A. L. Goldberger, R. Mueller, M. Kim, M. Rueschman, D. Mobley, S. S. Sahoo, C. P. Jayapandian, L. Cui, M. G. Morrical, S. Surovec, G.-Q. Zhang, and S. Redline, “Scaling Up Scientific Discovery in Sleep Medicine: The National Sleep Research Resource,” *Sleep*, vol. 39, no. 5, pp. 1151–1164, 2016. DOI: [10.5665/sleep.5774](https://doi.org/10.5665/sleep.5774).
- [36] G.-Q. Zhang, L. Cui, R. Mueller, S. Tao, M. Kim, M. Rueschman, S. Mariani, D. Mobley, and S. Redline, “The National Sleep Research Resource: towards a sleep data commons,” *J. Am. Med. Informatics Assoc.*, vol. 25, no. 10, pp. 1351–1358, 2018. DOI: [10.1093/jamia/ocy064](https://doi.org/10.1093/jamia/ocy064).
- [37] Y. A. LeCun, L. Bottou, G. B. Orr, and K. R. Müller, “Efficient backprop,” in *Neural Networks: Tricks of the Trade*, ser. Lect. Notes Comput. Sci. vol 7700, G. Montavon, G. B. Orr, and K.-R. Müller, Eds., Springer Berlin Heidelberg, 2012. DOI: [10.1007/978-3-642-35289-8-3](https://doi.org/10.1007/978-3-642-35289-8-3).
- [38] V. Nair and G. E. Hinton, “Rectified Linear Units Improve Restricted Boltzmann Machines,” in *Proc. 27th Int. Conf. Mach. Learn.*, Haifa, Israel, 2010.

- [39] S. Ioffe and C. Szegedy, “Batch Normalization: Accelerating Deep Network Training by Reducing Internal Covariate Shift,” in *Proc. 32nd Int. Conf. Mach. Learn.*, Lille, France: JMLR, 2015. arXiv: [1502.03167 \[cs.LG\]](#).
- [40] K. Cho, B. van Merriënboer, D. Bahdanau, and Y. Bengio, “On the Properties of Neural Machine Translation: Encoder–Decoder Approaches,” in *Proc. SSST-8, Eighth Work. Syntax. Semant. Struct. Stat. Transl.*, Stroudsburg, PA, USA: Association for Computational Linguistics, 2014, pp. 103–111. DOI: [10.3115/v1/W14-4012](#).
- [41] J. Chung, C. Gulcehre, K. Cho, and Y. Bengio, “Empirical Evaluation of Gated Recurrent Neural Networks on Sequence Modeling,” 2014. arXiv: [1412.3555 \[cs.NE\]](#).
- [42] A. Vaswani, N. Shazeer, N. Parmar, J. Uszkoreit, L. Jones, A. N. Gomez, L. Kaiser, and I. Polosukhin, “Attention Is All You Need,” in *31st Conf. Neural Inf. Process. Syst. (NIPS 2017)*, Long Beach, CA, USA, 2017. arXiv: [1706.03762 \[cs.CL\]](#).
- [43] J. Devlin, M.-W. Chang, K. Lee, and K. Toutanova, “BERT: Pre-training of Deep Bidirectional Transformers for Language Understanding,” 2019. arXiv: [1810.04805v2 \[cs.CL\]](#).
- [44] D. Bahdanau, K. Cho, and Y. Bengio, “Neural Machine Translation by Jointly Learning to Align and Translate,” in *3rd Int. Conf. Learn. Represent. (ICLR 2015)*, San Diego, CA, USA, 2015. arXiv: [1409.0473 \[cs.CL\]](#).
- [45] A. N. Olesen, P. Jennum, E. Mignot, and H. B. D. Sorensen, “Deep transfer learning for improving single-EEG arousal detection,” 2020.
- [46] S. Chambon, V. Thorey, P. J. Arnal, E. Mignot, and A. Gramfort, “A Deep Learning Architecture to Detect Events in EEG Signals During Sleep,” in *2018 IEEE 28th Int. Work. Mach. Learn. Signal Process.*, Aalborg, Denmark: IEEE, 2018, pp. 1–6. DOI: [10.1109/MLSP.2018.8517067](#).
- [47] S. Chambon, V. Thorey, P. Arnal, E. Mignot, and A. Gramfort, “DOSED: A deep learning approach to detect multiple sleep micro-events in EEG signal,” *J. Neurosci. Methods*, vol. 321, pp. 64–78, 2019. DOI: [10.1016/j.jneumeth.2019.03.017](#).
- [48] W. Liu, D. Anguelov, D. Erhan, C. Szegedy, S. Reed, C.-Y. Fu, and A. C. Berg, “SSD: Single Shot MultiBox Detector,” in *Comput. Vis. – ECCV 2016*, B. Leibe, J. Matas, N. Sebe, and M. Welling, Eds., Cham, Switzerland: Springer, 2016, pp. 21–37. DOI: [10.1007/978-3-319-46448-0_2](#).
- [49] T.-Y. Lin, P. Goyal, R. Girshick, K. He, and P. Dollar, “Focal Loss for Dense Object Detection,” *IEEE Trans. Pattern Anal. Mach. Intell.*, vol. 42, no. 2, pp. 318–327, 2020. DOI: [10.1109/TPAMI.2018.2858826](#).
- [50] D. P. Kingma and J. Ba, “Adam: A Method for Stochastic Optimization,” 2014. arXiv: [1412.6980 \[cs.LG\]](#).